Mechanical Properties of Cellular Materials. I. Linear Analysis of Hexagonal Honeycombs

MOHAMMED SWELLAM,[1] SUNG YI,*[,2] M. FOUAD AHMAD,[3] and LEE M. HUBER[4]

[1]Department of Civil Engineering, Cairo University, Giza, Egypt, [2]School of Mechanical and Production Engineering, Nanyang Technological University, Singapore, [3]National Center for Supercomputing Applications, University of Illinois at Urbana–Champaign, Urbana, Illinois 61801, and [4]The Dow Chemical Company, Freeport, Texas 77540

SYNOPSIS

The purpose of this series of studies is to develop finite element computer models of the mechanical properties of cellular polymers, especially open cell foams. Using finite element methods, both the properties of the material making up the struts, as well as the geometrical structure of the cell, can be readily varied. The series of studies begins with two-dimensional hexagonal honeycombs because of their ease of analysis and comparison with previous works. Comparison of the present solutions and analytic ones have been conducted, and excellent agreement is obtained. The effects of cell dimensions, such as strut length, strut depth, and cell height, of irregular hexagons on the effective Young's modulus of foams were studied in the low strain and elastic regime. Load direction and cell geometry anisotropy effects are also investigated. In addition, the effects of friction model and the specimen size on the effective Young's modulus of the foam are studied. Nonuniform strut thickness was also a variable. The modulus effects of these variations in geometry ranged from minimal to highly significant and provide an understanding of geometry effects on foam performance.

INTRODUCTION

With the recent determination that chlorofluorocarbons deplete the ozone in the upper atmosphere, their use in the production of flexible urethane foam has been curtailed. This means that soft, low density foam using water and other non-CFC blowing agents must be developed. In addition, there is a need to understand the performance of the high-load-bearing foams used for carpet underlayment, for example, to increase load bearing capacity and durability under cyclic loading.

It is expected that the foam performance is affected both by the mechanical properties of strut materials as well as the geometry and topology of the foam cells. Mechanical properties of polymer foams strongly depend on the density, the polymeric materials of cell struts, and geometric network structures. Therefore, it is necessary to evaluate mechanical properties of such materials associated with parameters such as cell geometry and foam density.

Foam materials may be classified according to the following two type of cells: open-cell and closed-cell foams. The topology of a typical foam is quite complex; it consists mainly of a space-filling array of cells. Each cell is built up of triangular cross-sectional struts. These cells may be quite uniform or may be of varying size. While open-cell foams have their cavities connected, closed-cell foams have isolated cavities filled with trapped air. Different approaches have been used in analyzing the mechanical behavior of foam materials. A micrograph of a typical open cell urethane foam being modeled here is shown in Figure 1. Some researchers[1] viewed foam materials, es-

* To whom correspondence should be addressed.

Journal of Applied Polymer Science, Vol. 63, 383–393 (1997)
 CCC 0021-8995/97/030383-11

pecially the closed-cell and rigid foams, as composite materials. Consequently, they used the equations developed for composite materials to predict the behavior of foam materials. Others[2,3] viewed foam materials as a spatially periodic structure that has a repeated unit cell composed of struts (and/or plates) connected together. The later group of researchers employed beam theory in analyzing a single unit cell of the foam and subsequently expressed the Young's modulus (and other elastic properties) in terms of the dimensions of the unit cell. The structural models of Gibson and Ashby[2] and Warren and Kraynik[3] have been developed in order to estimate the mechanical properties of cellular materials. Two models were based on two different unit cells with different deformation mechanisms, and assumptions as will be shown later.

The effects of cell thickness and strut Young's modulus are important factors that must be considered in determining the Young's modulus of the cellular materials. For example, cell struts of foam materials are generated by packing spherical bubbles together, which are produced by diffusion of gases. The polyurethane polymer is expanded or blown by the carbon dioxide gases or other blowing agent. Therefore, as shown in Figure 2, the thicknesses of the struts are typically greater near the intersections than in the center. Analytic models have limitations to analyze the real materials since cell shapes are not uniform and material properties for each strut are nonhomogeneous.

In the present study, macroscopic deformation behavior of two-dimensional hexagonal honeycombs with various material properties and geometry is investigated in the low strain and elastic regime. Finite element analyses are employed to determine the effective elastic modulus of the foams.

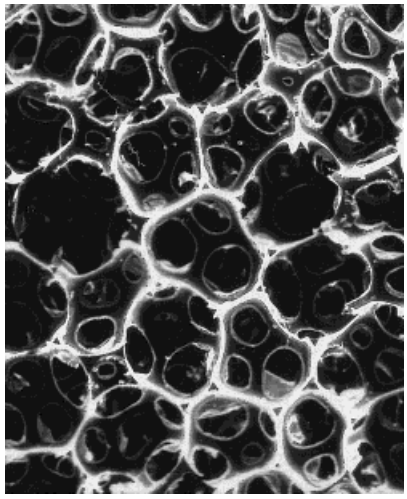

Figure 1 A micrograph of foam.

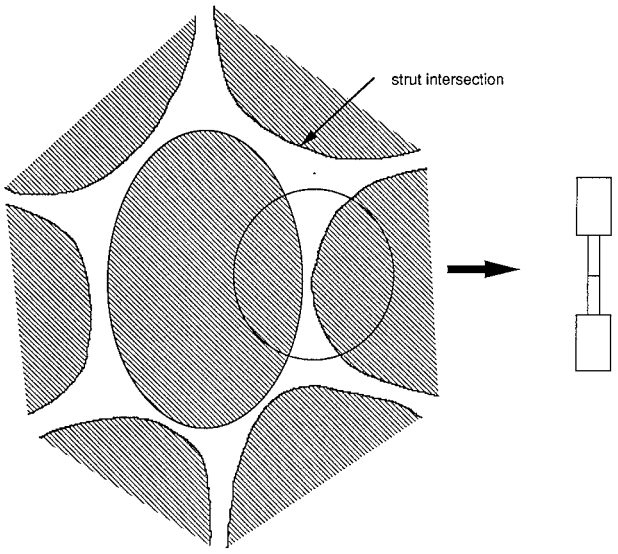

Figure 2 A schematic of foam.

ANALYSIS

Beam Theory

The equilibrium equations of a differential beam segment with its longitudinal axis coinciding with the X-axis of a Cartesian coordinate system and loaded with distributed longitudinal and transverse loads are given by the following:

$$\frac{dN}{dx} + F = 0 \tag{1}$$

$$\frac{dM}{dx} + Q = 0 \tag{2}$$

$$\frac{dQ}{dx} + S = 0 \tag{3}$$

where F and S are the components of the applied load in the axial and the perpendicular directions, respectively; N and Q are the normal and shear forces respectively; and M is the beam bending moment.

Geometric relations are as follows:

$$\varepsilon = \frac{du}{dx} \tag{4}$$

$$\kappa = \frac{d\theta}{dx} \tag{5}$$

$$b = \frac{dv}{dx} - \theta \tag{6}$$

where ε and β are the axial and shear strains; κ is the curvature in the plane; u and v are the displacements in the X and Y directions, respectively; and θ is the rotation in the X-Y plane.

Constitutive relations for linear elastic materials can be defined as follows:

$$N = EA\varepsilon \tag{7}$$

$$M = EI\kappa \tag{8}$$

$$Q = GA\beta \tag{9}$$

where A and I are the area and the first moment of inertia of the beam cross section, and G and E are the shear and Young moduli for the beam material.

If shear deformations are neglected (the shear strain $\beta = 0$), the equations reduces to those of the beam theory without shear deformations, which are given by the following:

$$\frac{d^2M}{dx^2} - S = 0 \tag{10}$$

$$\kappa = \frac{d^2v}{dx^2} \tag{11}$$

while the axial equations remain unchanged.

Structural Models

Several analytical models have presented for predicting the mechanical properties of the foam materials. Although such models employed Euler beam theory in analyzing the repeated unit cell of the spatially periodic structure, the different models were based on different deformation mechanisms and assumptions. The models of Gibson and Ashby[2] and Warren and Kraynik[3] represent two of the most common structural models that are based on two different deformation mechanisms.

Gibson and Ashby[2] presented a solution for the two-dimensional hexagonal honeycomb. They considered the bending deformations in the struts of one hexagonal cell, which they considered as the repeated unit cell (see Figs. 3 and 4). Invoking the equilibrium conditions, load-deformation relations, and the definition of the stiffness for the loadings in the X and Y directions, Gibson and Ashby[2] obtained the following:

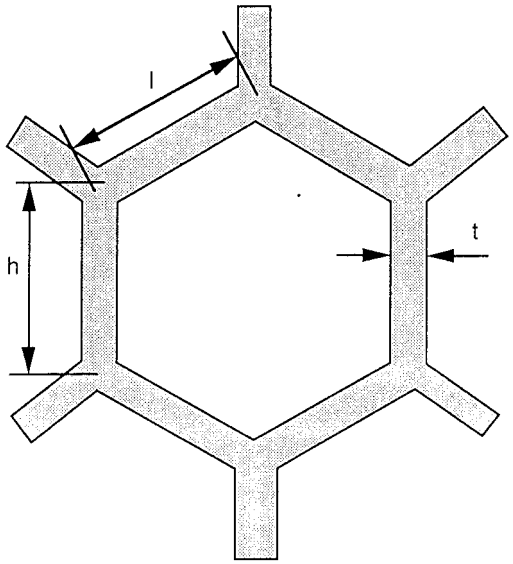

Figure 3 Geometry of honeycomb.

$$\frac{E_x}{E_s} = \left(\frac{t}{l}\right)^3 \frac{\cos\theta}{\left(\frac{h}{l} + \sin\theta\right)\sin^2\theta} \tag{12}$$

$$\frac{E_y}{E_s} = \left(\frac{t}{l}\right)^3 \frac{\left(\frac{h}{l} + \sin\theta\right)}{\cos^3\theta} \tag{13}$$

$$\mu_{xy} = \frac{\cos^2\theta}{\left(\frac{h}{l} + \sin\theta\right)\sin\theta} \tag{14}$$

$$\mu_{yx} = \frac{\left(\frac{h}{l} + \sin\theta\right)\sin\theta}{\cos^2\theta} \tag{15}$$

$$\frac{G_{xy}}{E_s} = \left(\frac{t}{l}\right)^3 \frac{\left(\frac{h}{l} + \sin\theta\right)}{\left(\frac{h}{l}\right)^2\left(1 + \frac{2h}{l}\right)\cos^3\theta} \tag{16}$$

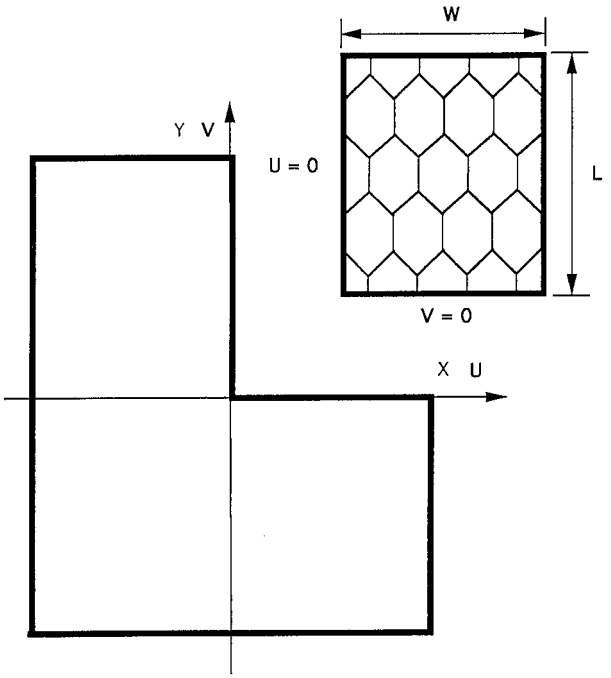

Figure 4 Finite element model.

where t is the strut depth, l is the length of inclined strut, h is the height of vertical strut, q is the strut inclination with the horizontal, E_s is the Young's modulus for the strut material, E_x is the Young's modulus for the foam material in the X-direction, E_y is the Young's modulus for the foam material in the Y-direction, G_{xy} is the shear modulus for the foam material in the X-Y plane, μ_{xy} is the Poisson's ratio for loading in the X-direction, and μ_{yx} is the Poisson's ratio for loading in the Y-dir.

It should be noted that Gibson and Ashby's model is limited to regular and irregular but geometrically similar hexagonal cells; for the regular hexagonal cells ($l = h$), the foam is transversely isotropic, and the above E_x and E_y solutions reduces to

$$\frac{E_x}{E_s} = \frac{E_y}{E_s} = 2.3\left(\frac{t}{l}\right)^3 \tag{17}$$

On the other hand, Warren and Kraynik[3] analyzed two-dimensional honeycombs of regular hexagons whose strut length is equal to 1. They applied the affine displacement theory to their repeated unit cell, which must deform in an antisymmetric fashion as dictated by the nature of the spatially periodic structure (see Fig. 4). The linear homogeneous deformation of unit cell is completely determined by the affine displacement of two strut midpoints with respect to the third strut midpoint. After invoking the load-displacement relations, equilibrium equations, compatibility conditions, and the elastic stress–strain relations of transversely isotropic materials, Warren and Kraynik[3] expressed the Young's modulus for honeycombs with regular hexagons as follows:

$$E_c = \frac{2}{\sqrt{3}(N + 3M)} \tag{18}$$

$$G_c = \frac{1}{2\sqrt{3}(N + M)} \tag{19}$$

$$\mu_c = \frac{(N - M)}{(N + 3M)} \tag{20}$$

For invariable strut depth,

$$M = \frac{L_1}{E_s t} \tag{21}$$

$$N = \frac{4L_1^3}{E_s t^3} \tag{22}$$

$$L_1 = \bar{L} - \frac{t}{2\sqrt{3}} \tag{23}$$

where E_s is the Young's modulus for the strut material, E_c is the in-plane Young's modulus for the transversely isotropic foam, G_c is the in-plane shear modulus for the transversely isotropic foam, μ_c is the in-plane Poisson's ratio for the transversely isotropic foam, and L is half of the strut length.

Finite Element Modeling of Foam Materials

The finite element approach is an alternative to the solution of the governing equations. In the finite element approach, the entire domain is divided into smaller elements; each element has its set of degrees of freedom (undetermined displacement components at the nodes of the element). These degrees of freedom are used in expressing the displacements fields over the element domain. The degrees of freedom are interpolated over the element domain with preselected approximate functions, usually polynomials. The equilibrium conditions lead to a system of equations that can

be expressed in a matrix form with the matrix of coefficients being the element stiffness matrix that multiplies the displacements.[4,5] The element stiffness matrix is calculated from the interpolation functions. The overall stiffness matrix of the structure is then assembled, and the system of equations for the whole structure are solved for the displacements (nodal degrees of freedom).

For beam elements without shear deformation, the element's essential nodal degrees of freedom are the end displacements perpendicular to the beam axis (provided that the axial deformations are neglected). The curvature is a second derivative of the displacements while the rotations are the first derivative. Thus, determining the displacements would be sufficient for subsequent determination of curvature and rotations. Nevertheless, a complete set of nodal degrees of freedom are usually used. The complete set of degrees of freedom include the end rotations as well as the end displacements. In such cases, the transverse displacement field over the element is expressed in terms of the interpolation (shape) functions, end rotations, and end displacements.

In the case of beam elements with shear deformations, the essential set of degrees of freedom includes the end rotations as well as end displacements; the rotations and the displacements are independent variables, as shown in eq. (6) of the shear strain. Hence, the rotations and displacements are interpolated separately. Interpolation functions for the displacements and rotations need not be of the same order since the rotations and the displacements are independent. Once the interpolation functions are determined, the stiffness matrix is formed, and the displacements and rotations are determined.

The general case of a framed structure in which the members are subjected to both axial and flexure deformations is handled by assuming the absence of any coupling between the axial and flexure stiffness mechanisms. The displacement fields within each element can be assumed as

$$u_i = N_{ij} q_j \tag{24}$$

where u_i is the generalized displacement vector, N_{ij} is interpolation function matrix, and q_j are nodal degrees of freedom.

The geometric relations can be found by differentiating the above with respect to the coordinate

$$\varepsilon_i = B_{ij} q_j \tag{25}$$

where ε_i is the generalized strain vector, and B_{ij} is strain-displacement matrix. By using the virtual work principle and eq. (25), the finite element formulation of a beam element can be obtained as the following:

$$K_{ij} U_j = P_i \tag{26}$$

where K_{ij} is global stiffness matrix, U_j is the global vector of nodal displacement, and P_i is global nodal force vector. More detail about the finite element formulation can be found in Bathe[4] and Hughes.[5]

Geometry and Boundary Conditions

Compression performance of polyurethane foams is of primary importance since cushioning involves mostly compressive loading. Some special requirements and limitations should be considered for the compression machine test. Loads must be applied flat and perpendicular to the axis of the specimen. There is friction between heads of the testing machine or bearing plates and the end surfaces of the specimen due to lateral expansion of the specimen. Usually, plain bearing plates are used to apply loads perpendicular to the specimen axis so as not to cause bending by eccentric loading.

To simulate the compression test of foam materials, all nodes on that surface are tied together with multiple point constraints in order to guarantee that all surface displacements perpendicular to the loaded surface should be equal. Friction between the heads of the testing machine or bearing plates and the end surfaces of the specimen is also modeled by multiple point constraints.

As shown in Figure 4, the X and Y axes are axes of symmetry. Consequently, if the nodes on the X and Y axes are restrained from moving in the X and Y directions, respectively, only the upper right quarter of the considered area can be analyzed. Moreover, the loaded nodes on the loaded surface were restrained from moving in the direction perpendicular to the loading direction and were also tied together (with multiple point constraints) such that all the loaded nodes displaced equally in the loading direction.

Young's Modulus Calculation from the Finite Element Analyses

The displacement of the loaded nodes ($\Delta_{f.e.}$) was used to calculate the Young's modulus ($E_{f.e.}$) of the analyzed area through the following equation:

$$E_{f.e.} = \frac{PH}{\Delta_{f.e.}A} \quad (27)$$

where $E_{f.e.}$ is the Young's modulus for the foam material calculated from the finite element; P is the applied load; H is the model height; and A is the model cross sectional area, which is perpendicular to loading direction.

It should be emphasized that in cases where the entire model width is loaded, the displacement of nodes on the loaded surface are guaranteed equal since all the nodes on that surface are tied with multiple point constraints.

RESULTS AND DISCUSSIONS

In most of the analyzed models, an area of 62.35 mm (model width, W) by 60 mm (model length, L) has been filled with two-dimensional hexagons; the characteristic dimensions of the unit cell varied from one model to another. The variation of the characteristic dimensions allows us to study the effects of the cell dimensions on the overall behavior of the analyzed area. Element breadth b (dimension perpendicular to the plane of the mesh) is equal to 0.05 mm.

Cubic Eulerian beam elements (element B23 in the ABAQUS finite element code[6]) of constant depth t are used to model the hexagons; each side was meshed by two elements. All elements possess the same depth except for those elements which are on the axis of symmetry; the depth of the elements on the axis of symmetry are half the regular depth. If regular hexagons of strut length to thickness ratios are less than ten, linear Timoshenko beam elements (element B21 in the ABAQUS finite element code[6]) are used. In such cases, the transverse shear effect may be significant.

Table I presents the geometry of models. The finite element model name indicates the number of cells in the horizontal and vertical directions of the model, respectively. The rc18 $\times$ 19 model is composed by 18 unit cells in X direction and 19 unit cells in Y direction. The length L and width W are the model dimensions in the X and Y directions, respectively.

Friction and Specimen Size Effects

Friction between heads of the testing machine or bearing plates and the end surfaces of the specimen due to lateral expansion of the specimen should be carefully considered for machine testing. In order to simulate such friction effect, multiple point constraints are applied to all nodes on the end surface of specimen. Friction factor is one with applied constraints and is zero without ones.

In this section, we study how such friction and the specimen size affect the effective Young's modulus of foams. Two loading conditions (vertical and horizontal) are considered, and five different size models (rc18 $\times$ 19, rc18 $\times$ 30, rc18 $\times$ 40, rc27 $\times$ 19, and rc32 $\times$ 19) are used. Geometric dimensions of unit cell and element breadth b are identical for all models. Finite element solutions without friction effect have a good agreement with Gibson and Ashby's results, as shown in Figures 5–8. Numerical studies show that the specimen size does not affect the effective Young's moduli of foam materials. However, the effective Young's moduli may be overestimated by friction effect during the test. Since increasing the dimension of surface perpendicular to loading axis increases friction force, increasing the end surface dimension significantly influences on the effective Young's modulus calculation. In order to minimize friction effect and errors on the effective Young's modulus evaluation caused by friction between heads of the testing machine or bearing plates and the end surfaces of the specimen, it is suggested that the end surface dimension should be smaller than other one.

Cell Dimensions Effects

Regular hexagonal cells with the same strut depth (t = 0.05 mm) are used to fill the 62.35 $\times$ 60 area (actual F.E. model dimensions are half these values, 31.17 $\times$ 30.00, after considering the symmetry conditions). Four models (rd36 $\times$ 39, rc18 $\times$ 19, rb12 $\times$ 13, and ra9 $\times$ 9) are analyzed. In this case, side length and cell height are changed simultaneously by the identical ratio. Figure 9 shows that the effective Young's modulus of the foam decreases with the increase of cell side length and cell side height. An increase in the cell side length from 0.5 to 1. mm resulted in a decrease in the effective Young's modulus value from 458 to 57.5 MPa. A further increase in the side length to 2 mm has decreased the value to about 7 MPa. Similar trends are also observed for the Young's modulus values calculated from Gibson's and Kraynik's models. Figures 9 and 10 show the good agreement between the finite element results and the other two models. From the material point of view, the decrease in the foam

Table I Finite Element Models

EE Model	Length (mm)	Width (mm)	l (mm)	h (mm)
ra9 × 9	30.000	31.176	2.00	2.00
rb12 × 13	31.500	31.176	1.50	1.50
rc18 × 19	30.000	31.176	1.00	1.00
rc18 × 29	45.000	31.176	1.00	1.00
rc18 × 39	60.000	31.176	1.00	1.00
rc27 × 19	30.000	46.764	1.00	1.00
rc32 × 19	30.000	46.764	1.00	1.00
rd36 × 39	30.000	31.176	0.50	0.50
ih18 × 9	30.000	31.176	1.00	2.50
ih18 × 11	30.000	31.176	1.00	2.00
ih18 × 15	30.000	31.176	1.00	1.37
ih18 × 23	30.000	31.176	1.00	0.75
ih18 × 29	30.000	31.176	1.00	0.50
ih18 × 39	30.000	31.176	1.00	0.25

relative density usually yields a decrease in the Young's modulus value. The Young's modulus values versus normalized density to the power 3 are plotted in Figure 10.

Loading Direction and Cell Geometric Anisotropy Effects

The horizontal and vertical values of the Young's moduli for the rc18 × 19 model are not significantly different (57.55 and 56.46 MPa, respectively). This insignificant difference in the Young's moduli is due to this model having regular hexagonal cells with $l/h = 1$. In other situations where the l/h ratio is not equal to one (irregular hexagonal cells), the calculated Young's modulus value is found to vary significantly with the loading direction.

Models ih18 × 9, ih18 × 11, ih18 × 15, ih18 × 23, ih18 × 29, and ih18 × 39 (all these models

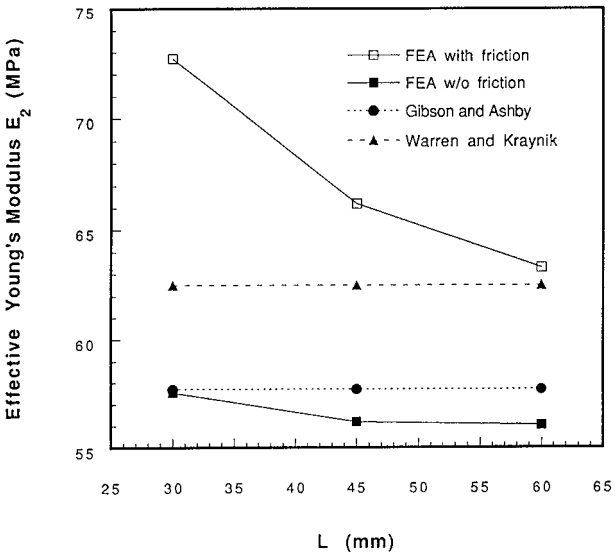

Figure 5 Effective Young's modulus E_2 of honeycombs with regular hexagons versus foam height L: (⊟) FEA with friction; (■) FEA without friction; (· · · ● · · ·) Gibson and Ashby[2]; (– – ▲ – –) Warren and Kraynik.[3]

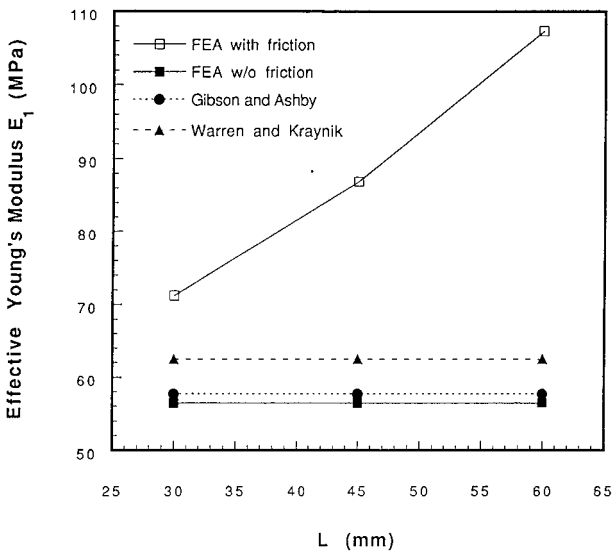

Figure 6 Effective Young's modulus E_1 of honeycombs with regular hexagons versus foam height L: (⊟) FEA with friction; (■) FEA without friction; (· · · ● · · ·) Gibson and Ashby[2]; (– – ▲ – –) Warren and Kraynik.[3]

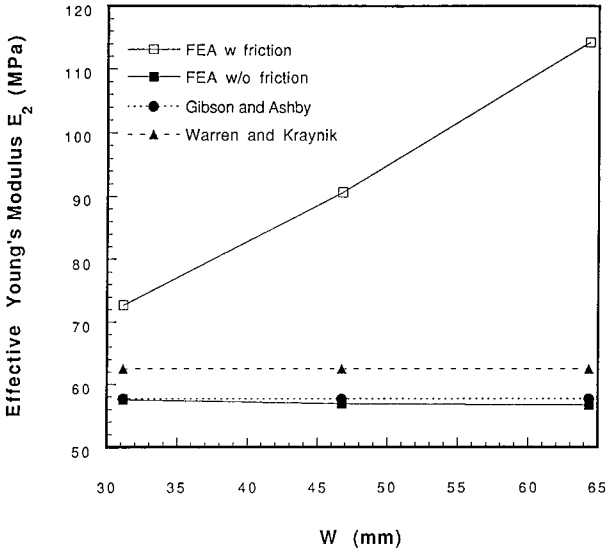

Figure 7 Effective Young's modulus E_2 of honeycombs with regular hexagons versus foam width W: (⊟) FEA with friction; (■) FEA without friction; (· · · ● · · ·) Gibson and Ashby[2]; (– – ▲ – –) Warren and Kraynik.[3]

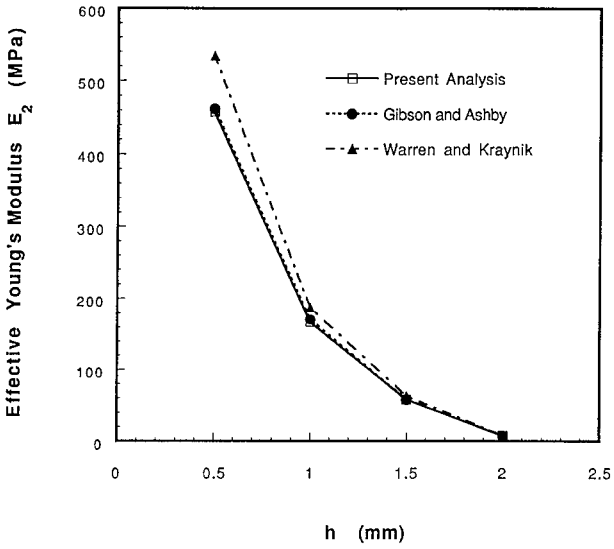

Figure 9 Effect of cell size on the effective Young's modulus of honeycombs with regular hexagons: (⊟) present analysis; (· · · ● · · ·) Gibson and Ashby[2]; (– – ▲ – –) Warren and Kraynik.[3]

have the same area of $62.35 \times 60.\ \text{mm}^2$) are used for studying the influence of the cell height and irregularity of cell shape on the effective Young's moduli of foams. The length of the inclined strut ($l = 1.$ mm), the strut depth ($t = 0.05$ mm), and the model area are identical for all models. The cell height is varied from one model to another, and all models are loaded in the vertical direction (cell height direction) or the horizontal direction.

The influence of the cell height on the subse-

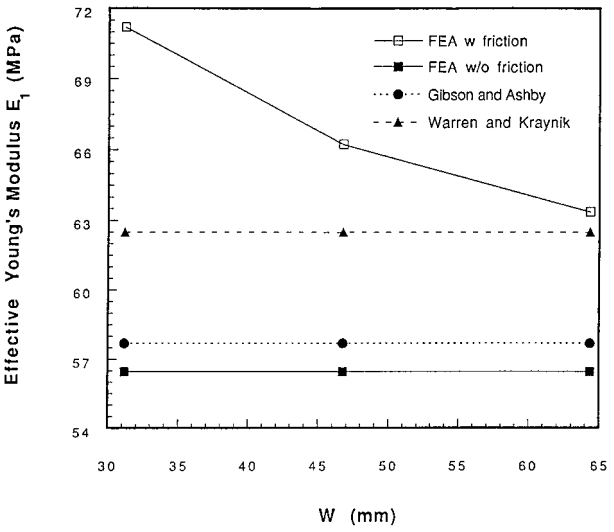

Figure 8 Effective Young's modulus E_1 of honeycombs with regular hexagons versus foam width W: (⊟) FEA with friction; (■) FEA without friction; (· · · ● · · ·) Gibson and Ashby[2]; (– – ▲ – –) Warren and Kraynik.[3]

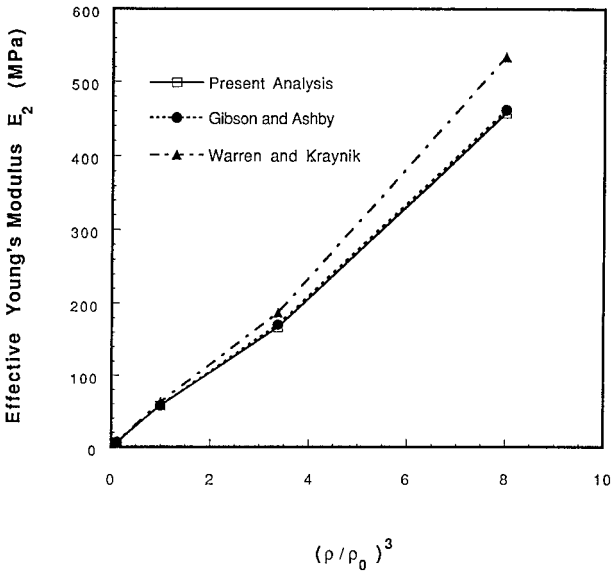

Figure 10 Effective Young's modulus of honeycombs with regular hexagons versus cube of density: (⊟) present analysis; (· · · ● · · ·) Gibson and Ashby[2]; (– – ▲ – –) Warren and Kraynik.[3]

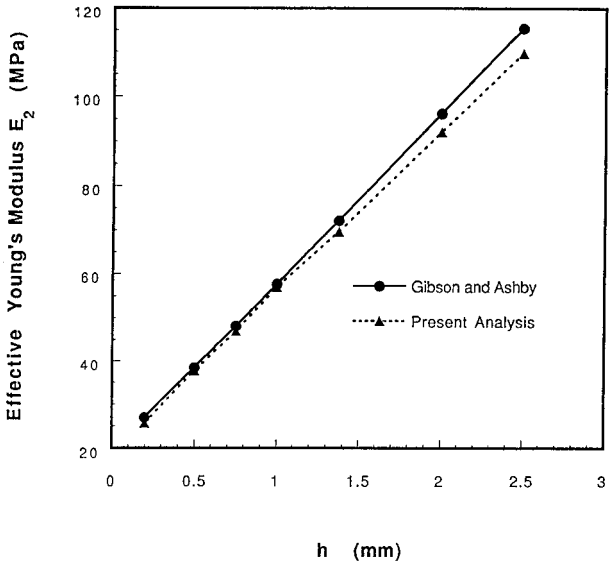

Figure 11 Effective Young's modulus E_2 of honeycombs with irregular hexagons versus cell height: (-●-) Gibson and Ashby[2]; (– – – – ▲ – – – –) present analysis.

quent Young's moduli is illustrated in Figures 11 and 12. The study shows that the increase of cell height increases the effective Young's modulus values for the vertical load while it decreases the effective Young's modulus values for the horizontal load. It should be noted that Kraynik's

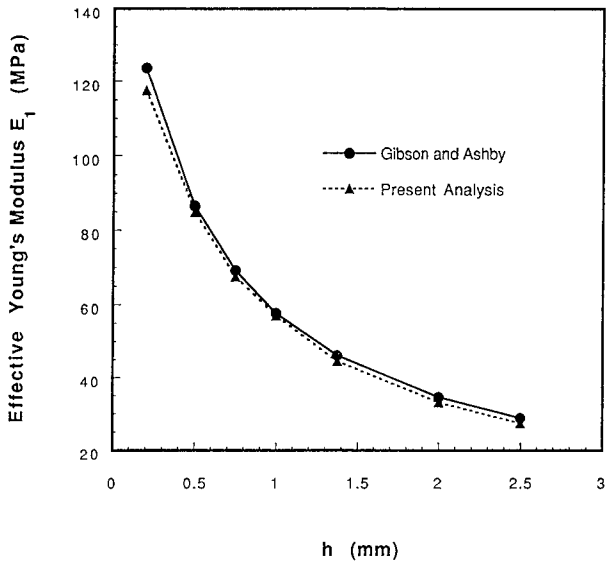

Figure 12 Effective Young's modulus E_1 of honeycombs with irregular hexagons versus cell height: (-●-) Gibson and Ashby[2]; (– – – – ▲ – – – –) present analysis.

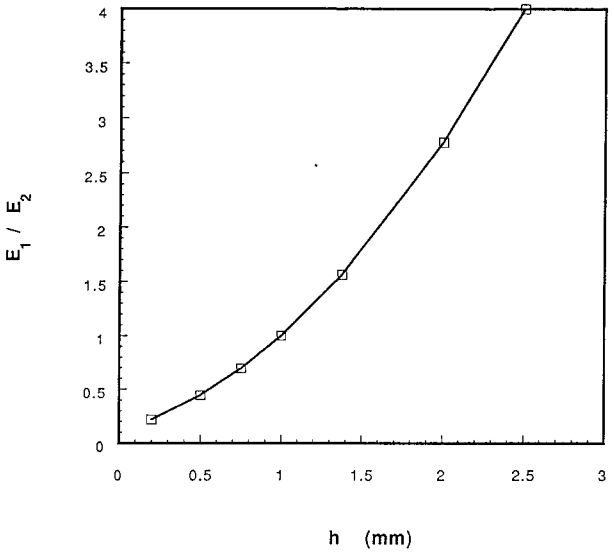

Figure 13 E_1/E_2 of honeycombs versus cell height.

model does not evaluate the effective Young's modulus for non-regular hexagonal cells, as in ih18 × 9, ih18 × 11, ih18 × 15, ih18 × 23, ih18 × 29, and ih18 × 39. Gibson and Ashby's model shows a small discrepancy with the present finite element solution, which increases at large cell height. As shown in Figure 13, the anisotropy in cell geometry increases anisotropy of foam materials.

The previous study with regular hexagonal cells and experimental results show that the decrease in the foam relative density yields a decrease in the Young's modulus value. However, as illustrated in Figure 14, the effective Young's modulus values for the vertical loading decrease with respect to increasing foam density. The material argument fails to explain the above trend where increasing the cell height results in a decrease in the foam relative density, i.e., the material argument generally predicts a decrease in the Young's modulus with the increase in cell height. On the other hand, the structural argument differentiates between the following two cases: case 1, in which a vertical load is applied; and case 2, in which a horizontal load is applied. While the Young's modulus increases with the increase in cell height for case 1, the Young's modulus decreases with the increase of cell height in case 2. This behavior can be explained in terms of the relative axial and bending stiffness of foams.

These results suggest how to best manufacture the foam material to increase the load bearing

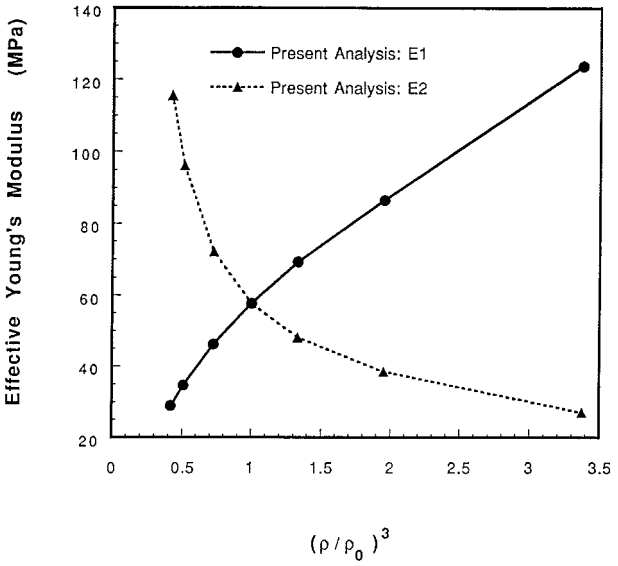

Figure 14 Effective Young's moduli of honeycombs with irregular hexagons versus cube of density. (-●-); Present analysis: E1; (– – – –▲– – – –) present analysis: E2 .

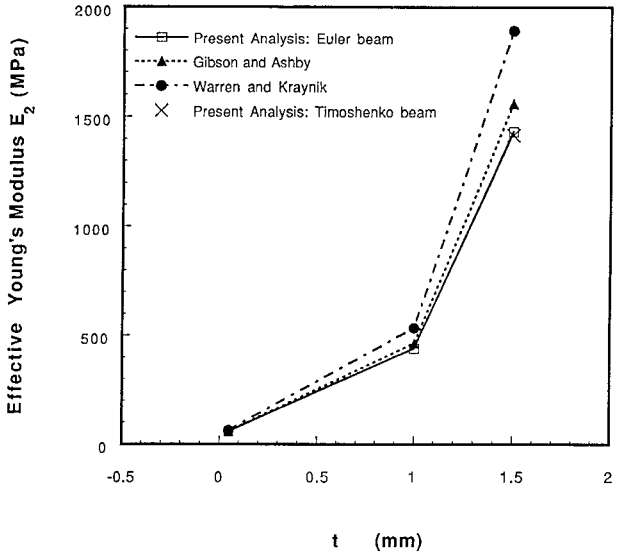

Figure 15 Effective Young's modulus E_2 of honeycombs with regular hexagons versus strut depth. (-⊟-) Present analysis: Euler Beam (----▲----) Gibson and Ashby[2]; (– – ● – –) Warren and Kraynik[3]; (×) present analysis: Timoshenko Beam.

ability with minimum structural weight for specific service condition.

Strut Depth Effect

The strut depth effect is similarly studied through the analyses of the c18 × 19 model. Three different thicknesses, 0.05, 0.1, and 0.15 mm, are considered with regular hexagon elements. Figure 15 shows that an increase in strut depth results in an increase in the effective Young's modulus value; the finite element Young's modulus value increased from 57.5 to 1432 MPa. In Figure 15, the finite element results are compared with the Gibson and Ashby's and Warren and Kraynik's models. The results for the finite element analyses and Gibson and Ashby's model are in good agreement. However, about 25% discrepancy between finite element results and the Warren and Kraynik's model is observed for the case with the largest thickness. In the last case, the $2L/t$ ratio is 6.7, and the Timoshenko beam elements are used for the analysis in order to account for the transverse shear effect. A little bit smaller value 1417 MPa is obtained for the vertical effective Young's modulus.

As illustrated in Figure 16, the increase of strut thickness results in the increase of the relative density of the foam and the increase of effective Young's modulus. The structural and the material arguments agree on the increase in the Young's modulus with the increase in the strut depth.

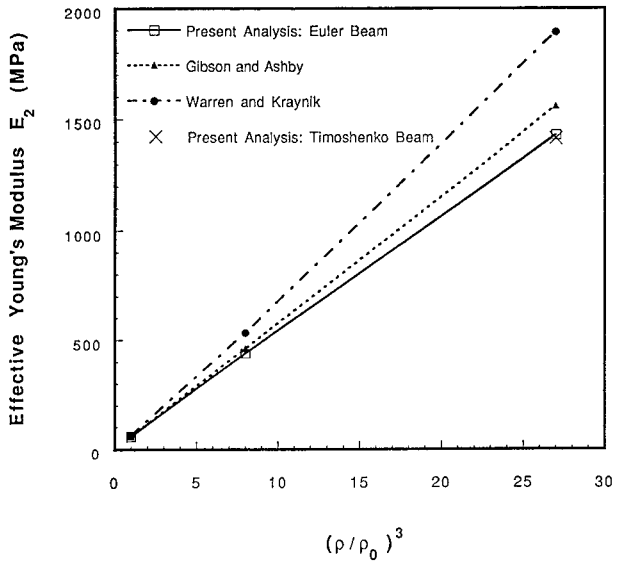

Figure 16 Effective Young's modulus E_2 of honeycombs with various strut depths versus cube of density. (-⊟-) present analysis: Euler beam; (----▲----) Gibson and Ashby[2]; (– – ● – –) Warren and Kraynik[3] (×) present analysis: Timoshenko beam.

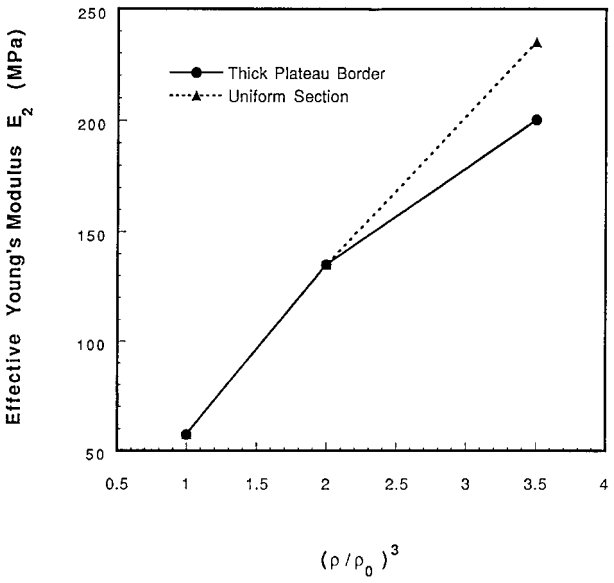

Figure 17 Effective Young's modulus E_2 of honeycombs with uniform strut section and thick strut intersection: (-●-) thick plateau border; (----▲----) uniform section.

Strut Intersection Thickness Effect

In this section, we observe the effect of the thickness at the intersection on macroscopic mechanical properties of the foams. The thicknesses at the intersection are taken as 0.05, 0.075, and 0.1 mm. As shown in Figure 17, results for uniform sections are compared with ones for varied sections. For both cases, foam densities remain identical. Results show that effective stiffnesses for both cases are almost the same up to density ratio = 2. However, significant discrepancy is observed for the 0.1 mm case.

SUMMARY

- Finite element techniques can be utilized to characterize the mechanical properties of the foam materials.
- The effective Young's modulus decreases with the increase of the length of the unit cell side l and cell height h and with the decrease of foam density.
- The effective Young's modulus increases with the increase of the strut depth as well as cell height.
- There was no significant change in the effective Young's modulus with respect to foam dimensions and model aspect ratio.
- Study shows that friction between heads of the testing machine or bearing plates and the end surfaces of the specimen due to lateral expansion of the specimen should be carefully considered for machine testing. Since increasing the dimension of surface perpendicular to loading axis increases friction force, then increasing end surface dimension significantly influences the effective Young's modulus calculation.
- Results for uniform sections are compared for ones with varied strut intersections. For both cases, foam densities remain identical. Results show that effective stiffnesses for both cases are almost the same up to density ratio = 2. However, significant discrepancy is observed above that ratios.
- The effect of the loading direction on the effective Young's modulus is due to anisotropic nature of foams, and such anisotropy in foams reflects the anisotropy in cell structural geometry and in the cell materials.

REFERENCES

1. N. C. Hilyard, *Mechanics of Cellular Plastics,* 1982.
2. L. J. Gibson and M. F. Ashby, *Cellular Solids, Structure and Properties,* Pergamon Press, Elmsford, New York, 1988.
3. W. E. Warren and A. M. Kraynik, "Foam Mechanics: The Linear Elastic Response of Two Dimensional Spatially Periodic Cellular Materials," *Mech. of Materials,* Vol. 6, 1987, pp. 27–37.
4. K. Bathe, *Finite Element Procedures in Engineering Analysis,* Prentice-Hall, New York, 1982.
5. T. Hughes, *The Finite Element Method,* Prentice-Hall, New York, 1987.
6. ABAQUS, *User's Manual,* Version 5.3, 1993, Hibbitt, Karlsson and Sorensen, Inc.

Received January 11, 1996
Accepted June 1, 1996